

Article

# Identification of Typical Sub-Health State of Traction Battery Based on a Data-Driven Approach

Cheng Wang <sup>1,2</sup>, Chengyang Yu <sup>3</sup>, Weiwei Guo <sup>3,\*</sup>, Zhenpo Wang <sup>1</sup> and Jiyuan Tan <sup>3</sup>

<sup>1</sup> National Engineering Laboratory for Electric Vehicles, School of Mechanical Engineering, Beijing Institute of Technology, Beijing 100000, China; wang\_ch@126.com (C.W.); wangzhenpo@bit.edu.cn (Z.W.)

<sup>2</sup> Beijing CATARC Science and Technology Center Co., Beijing 100000, China

<sup>3</sup> Beijing Key Lab of Urban Intelligent Traffic Control Technology, North China University of Technology, Beijing 100000, China; ccy131100205262022@163.com (C.Y.); tjyphilip@163.com (J.T.)

\* Correspondence: guoweiwei@ncut.edu.cn

**Abstract:** As the core component of an electric vehicle, the health of the traction battery closely affects the safety performance of the electric vehicle. If the sub-health state cannot be identified and dealt with in time, it may cause traction battery failure, pose a safety hazard, and cause property damage to the driver and passengers. This study used data-driven methods to identify the two typical types of sub-health state. For the first type of sub-health state, the interclass correlation coefficient (ICC) method was used to determine whether there was an inconsistency between the voltage of a single battery and the overall voltage of the battery pack. In order to determine the threshold, the ICC value of each vehicle under different working conditions was analyzed using box plots, and a statistical ICC threshold of 0.805 was used as the standard to determine the first sub-health type. For the second type of sub-health state, the Z-score and the differential area method were combined to determine whether the single cell voltage deviated from the overall battery pack voltage. A battery whose voltage differential area exceeds the range of  $u \pm 3\sigma$  is regarded as having a sub-health state. The results show that both methods can accurately judge the sub-health state type of a single battery. Furthermore, combined with the one-month operation data of the vehicle, we could calculate the sub-health state frequency of each single battery and take single batteries with a high frequency as the key object of attention in future vehicle operations.

**Keywords:** data driven; sub-health state; ICC; differential area; box plot; Pauta criterion



**Citation:** Wang, C.; Yu, C.; Guo, W.; Wang, Z.; Tan, J. Identification of Typical Sub-Health State of Traction Battery Based on a Data-Driven Approach. *Batteries* **2022**, *8*, 65. <https://doi.org/10.3390/batteries8070065>

Academic Editors: Binghe Liu, Lubing Wang, Yuqi Huang, Yongjun Pan, Carlos Ziebert and Pascal Venet

Received: 14 March 2022

Accepted: 28 June 2022

Published: 4 July 2022

**Publisher's Note:** MDPI stays neutral with regard to jurisdictional claims in published maps and institutional affiliations.



**Copyright:** © 2022 by the authors. Licensee MDPI, Basel, Switzerland. This article is an open access article distributed under the terms and conditions of the Creative Commons Attribution (CC BY) license (<https://creativecommons.org/licenses/by/4.0/>).

## 1. Introduction

In recent years, with the popularization of electric vehicles (EVs), more and more problems have been exposed during their use [1]. Finding out how to make significant developments to EVs has thus become an urgent problem to be solved [2]. Compared to traditional vehicles, the power batteries of EVs have the characteristics of high heat generation, multiple electrical circuits, and complex control systems during use and charge-discharge. As the core component of EVs [3,4], traction battery systems can not only provide power output and braking energy recovery, but also greatly affect the driving safety and cruising range of EVs [5,6]. Although the research and development of traction batteries and the production technology of traction batteries are making continuous progress, the management strategy of traction batteries still needs to be improved [7,8]. Based on the driver's operation and various factors, the traction battery system, cell, or related components will be damaged to varying degrees and enter a sub-health state during use [9]. If the sub-health state cannot be identified and dealt with in time, it may cause traction battery failure, pose a safety hazard, and cause property damage to the driver and passengers. According to incomplete statistics, there were more than 124 electric vehicle fire accidents in China in 2020, and nearly half of them occurred in July, August, and September.

The causes of the accidents included the imperfect control strategy of the current battery management system (BMS), improper use by the operators, poor environmental conditions, etc. [10,11]. Therefore, the real-time monitoring and diagnosis of the health status of the traction battery throughout its life cycle are particularly important.

At present, in order to ensure the safety and reliability of EVs and reduce the accident rate caused by the failure of the traction battery system, domestic and international scholars are committed to studying fault diagnosis methods for traction batteries [12,13]. Commonly used traction battery fault detection methods include the threshold method, the empirical model method, and machine learning methods [14].

Vehicle manufacturers and traction battery management system manufacturers have set different fault levels, which mainly diagnose some simple and obvious battery faults. To build on this, Chen et al. [15,16] proposed an improved threshold method which calculates the voltage difference between any two terminal voltages and compares the maximum value of the voltage difference with the threshold. When the difference exceeds the threshold, the fault detection mechanism will alert the user. Han et al. [17] set a specific voltage threshold, calculated the voltage change value of a battery pack continuously discharged with 1 C current for a fixed period of time, and made a diagnosis by comparing the threshold value with the measured value. Xia et al. [18] proposed a short-circuit fault alarm based on temperature change rate, voltage threshold, and current threshold. The difficulty of the threshold method is in setting a reasonable threshold. If the threshold is too small, alarms will be issued frequently, and if the threshold is too large, the fault cannot be detected in time.

For empirical modeling methods, many scholars have studied model simulation. Chen et al. [19] proposed a synthesized design of reduced-order Luenberger observers and LOs for the purpose of simultaneous fault isolation and estimation of a three-cell battery string. The number of batteries used in the study of this method was small, and the possibility of applying it to a multi-cell battery pack is not high. Xu et al. [20] used a first-order RC equivalent circuit model to analyze the contact failure of a battery pack, used the least square method to identify the model parameters, and analyzed the cause of the battery failure through Simscape simulation. Sidhu et al. [21] estimated the residual signal generated by the terminal voltage by extending the Kalman filter and applied it to the multi-model adaptive estimations technology to generate a certain characteristic failure probability to diagnose battery failures. Liu et al. [22] established a battery model through equivalent circuit technology and proposed a battery fault diagnosis scheme to detect faults in current or voltage sensors. Dey et al. [23] used an equivalent circuit model and a thermal model to estimate current, voltage, and temperature, generated residuals using three synovial film observers, and finally realized fault detection and isolation of the voltage sensor, current sensor, and temperature sensor. Tran et al. [24] used a simulation framework based on a battery voltage model and a degradation model to investigate the feasibility and benefits of the battery replacement concept. Chen et al. [25] presented a multi-fault diagnosis approach based on a hybrid system for diagnosing cell parametric faults, sensor faults, and relay faults in a Li-ion battery pack. Hu et al. [26] proposed a novel ISC diagnostic method which uses, for the first time, recursive total least squares with variable forgetting (RTLS-VF) to mitigate the adverse effects of measurement disturbances. These studies are still based on model simulation and were rarely verified by experiments. In the actual application in EVs, the accuracy of fault diagnosis will have a certain deviation.

In recent years, with the gradual development of machine learning, research on fault diagnosis based on machine learning has become more and more frequent. Hong et al. [27] proposed a multi-step accurate prediction method of battery system voltage based on deep learning, which is the first application of LSTM to voltage failure prediction in a battery system. However, this method requires one-year operation data of vehicles, which has high requirements on the time dimension of the sample size. Yao et al. [14] proposed a fault detection method for lithium-ion batteries based on a wavelet neural network based on the decomposition and reconstruction of discrete wavelet transform

(DWT) to eliminate voltage signal noise. However, the required data sample size directly affects the method accuracy. Yang et al. [28] used the two characteristics of maximum temperature rise and minimum discharge capacity of leaking batteries and proposed a method based on the random forest (RF) classifier to effectively classify normal and faulty batteries and accurately diagnose external short-circuit faults. This method requires a lot of training data. Gao et al. [29] established a single hidden layer back-propagation neural network optimized by the genetic algorithm to diagnose battery faults. However, this method directly regards the total voltage as the research object, without considering the relationship between the single battery modules. Xia et al. [30] used BP and RBF neural networks to make a preliminary diagnosis of lithium battery fault feature vectors based on the complexity and uncertainty of lithium battery faults in EVs. Then, they used the combination rules of the D-S evidence theory to fuse the evidence bodies of different neural networks and the weighted evidence bodies to diagnose battery faults. However, due to the use of multiple models, the algorithm was too complicated, and the calculation efficiency was low. Although the machine learning method has a high accuracy, its accuracy is affected by the sample size and noise, and applicability to EVs in actual operation is difficult to achieve.

In summary, the current battery pack fault diagnosis methods have shortcomings in different aspects in practical applications. Li et al. [31] used an ICC to advance fault resolution by amplifying the voltage difference, and to determine whether the battery is short-circuited. However, it is necessary to sequentially compare the size of the ICC between the cell voltages when determining this, and without considering the consistency of the voltage data, 0.75 was directly selected as the ICC threshold. In the work of Xue et al. [32], although the  $3\sigma$  multi-level screening strategy was used to determine the fault, it did not consider the instantaneous rise in the voltage due to emergency operations. A certain process is required for a battery to change from a healthy state to a faulty state. For this reason, this article uses the term “sub-health state” to study the battery state. This paper analyzes two potential sub-health states based on a data-driven method. The ICC, Z-score, and differential area methods are used to identify the two sub-health states, and the method is verified using vehicle voltage data under different working conditions.

## 2. Voltage Data Analysis

### 2.1. Data Introduction and Preprocessing

The operating data of EVs mainly include the traction battery system, motor drive system, vehicle control system, and other parts. The parameter data of the traction battery system mainly include the total voltage and current of the battery system, the SOC state, the battery cell voltage, the temperature of the characteristic points of the battery pack, etc.

During the actual operation of EVs, due to the variability and unpredictability of factors such as road conditions and driving behavior, the battery voltage will also fluctuate sharply [27]. The vehicles we studied were 72 pure EVs equipped with lithium-ion battery packs from the Open Lab of the National Big Data Alliance for New Energy Vehicles, a non-shareable online data platform. The specific parameters are shown in Table 1. Real-time monitoring data were transmitted through the network. There was a delay in the transmission process, which caused problems such as data loss, abnormality, duplication, and an inconsistent sampling frequency. Therefore, it was necessary to delete duplicate values and then identify and delete abnormal values according to the technical specifications. Due to the small data transmission interval, the missing values could be filled with the upper and lower mean values. Finally, the obtained data were resampled at 0.1 Hz.

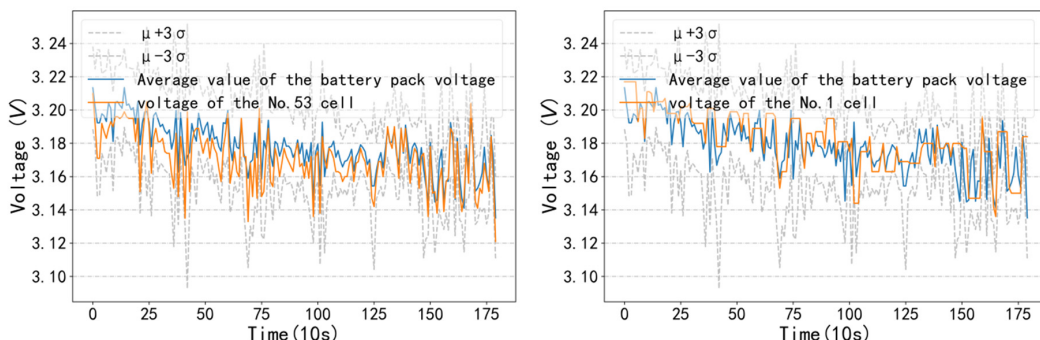
**Table 1.** Specific parameters of the vehicle.

Vehicle Type	Pure Electric Vehicle
Curb weight (kg)	2420
Energy consumption per hundred kilometers (kwh/100)	20.5
Maximum speed (km/h)	155
Rated total energy of battery (kwh)	82

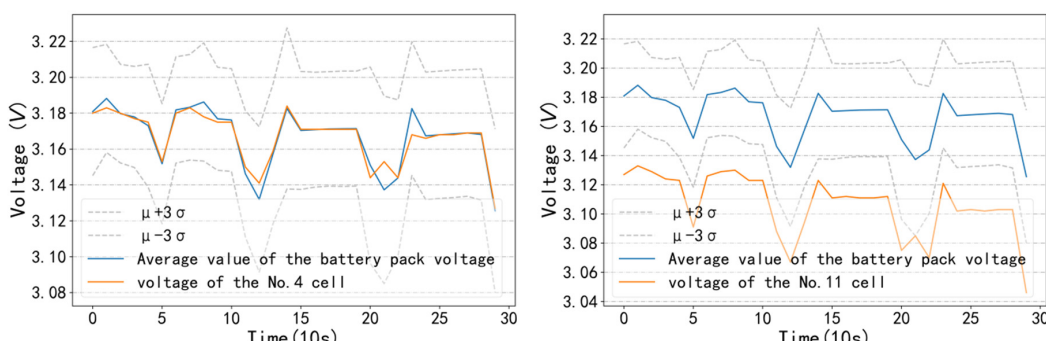
## 2.2. Types of Sub-Health Status

The power battery consists of multiple single cells in series and parallel combination. The specifications and models of each single cell in the system are identical, so in theory, they all have rotation symmetry. According to the characteristics of series and other flow, the change trend and range of the single cell voltage are consistent [33,34]. The average voltage of the single cells in a battery pack represents the concentration of the battery pack voltage, which can reflect the overall trend of the battery pack voltage. In order to analyze the consistency of the single-cell voltage and the overall voltage of the battery pack, the single-cell voltage ( $V$ ) was compared with the average value of battery pack voltage ( $\bar{V}$ ). By analyzing the real-time monitoring voltage data of electric vehicles, two types of battery sub-health status could be summarized.

Battery sub-health state type I: The voltage of the single cell is inconsistent with the overall voltage of the battery pack. As shown in Figure 1, compared with the voltage of single cell No. 53 on the left, the voltage of cell No. 1 on the right has an inconsistent change with the overall voltage of the battery pack.

**Figure 1.** Battery sub-health state type I (graph of the voltage of the single battery over time).

Battery sub-health state type II: The voltage of the single battery deviates from the overall voltage of the battery pack. As shown in Figure 2, compared with the voltage of single battery No. 4 on the left, the voltage of single battery No. 11 on the right deviates from the overall voltage of the battery pack and exceeds the  $3\sigma$  range.

**Figure 2.** Battery sub-health state type II (graph of the voltage of the single battery over time).

### 3. Identification of Sub-Health Status

#### 3.1. Identification Algorithm of Sub-Health State Type

##### 3.1.1. ICC

The ICC method can evaluate both quantitative data and the reliability of classified data [35]. Its value is between 0 and 1. It is generally believed that a reliability coefficient lower than 0.4 indicates poor reliability, and a reliability coefficient greater than 0.75 indicates good reliability [36,37]. The sub-health state of the battery Type I is that the trend of the voltage of the single cell is inconsistent with the average voltage of the battery pack and does not change with the average voltage of the battery pack at some time, or even changes with a delay. To show this inconsistency, we took the cell voltage difference between adjacent time points in the  $j$ -th column ( $V_{j,diff}$ ) as one group and used the overall battery voltage average difference between adjacent time points ( $\bar{V}_{diff}$ ) as another group.

$$ICC = \frac{(MS_{bl} - MS_{er})/m}{(MS_{bl} - MS_{er})/m + MS_{er}} \quad (1)$$

In Formula (1),  $MS_{bl}$  is the mean square error of the block term,  $MS_{er}$  is the mean square error of the error term, and  $m$  is the number of treatment groups.

$$MS_{er} = \frac{SS_{er}}{v_{er}}, \quad (2)$$

$$MS_{bl} = \frac{SS_{bl}}{v_{bl}}, \quad (3)$$

where  $SS_{bl}$  and  $SS_{er}$  represent the sum of squares of deviation from the mean, and  $v_{bl}$  and  $v_{er}$  represent the degrees of freedom.

$$v_{bl} = b - 1, \quad (4)$$

$$v_{er} = (k - 1)(b - 1), \quad (5)$$

$$SS_{bl} = \sum_{i=1}^b \frac{\left(\sum_{j=1}^k x_{ij}\right)^2}{k} - C, \quad (6)$$

$$SS_{tr} = \sum_{j=1}^k \frac{\left(\sum_{i=1}^b x_{ij}\right)^2}{b} - C, \quad (7)$$

$$SS_{er} = \sum x^2 - SS_{bl} - SS_{tr} - C, \quad (8)$$

where  $b$  is the number of blocks,  $k$  is the number of treatment groups,  $x_{ij}$  represents the data of the  $i$ -th row and the  $j$ -th column, and  $C$  is the calculated correction coefficient.

$$C = \frac{(\sum x)^2}{N}, \quad (9)$$

where  $N$  is the total number of data points.

##### 3.1.2. Z-Score

The Z-score, also called the standard score, is the result of dividing the difference between a number and the mean by the standard deviation, which can reflect the relative standard distance between the sample and its mean. Due to the consistency of a single battery, the voltage of each single battery fluctuates within a certain range, and the Z-score can determine the degree of dispersion of the voltage of each single battery. The

sample is composed of instantaneous cell voltage, and the calculation model is shown in Formula (10).

$$Z_{i,j} = \frac{x_{i,j} - \mu_i}{\sigma_i}, \quad (10)$$

where  $Z_{i,j}$  is the Z-score of the  $j$ -th single battery's voltage at the  $i$ -th time point, and  $x_{i,j}$  is the  $j$ -th single battery's voltage at the  $i$ -th time point.

$$\sigma_i = \sqrt{\frac{1}{n} \left[ \sum_{j=1}^n (x_{i,j} - \mu_i)^2 \right]}, \quad (11)$$

where  $\sigma_i$  is standard deviation of the battery pack voltage at the  $i$ -th time point, and  $\mu_i$  is the average value of battery pack voltage at the  $i$ -th time point.

$$\mu_i = \frac{1}{n} \sum_{j=1}^n (x_{i,j}), \quad (12)$$

$$Z_{i,j} = \frac{x_{i,j} - \frac{1}{n} \sum_{j=1}^n (x_{i,j})}{\sqrt{\frac{1}{n} \left[ \sum_{j=1}^n (x_{i,j} - \mu_i)^2 \right]}}, \quad (13)$$

### 3.1.3. Differential Area Method

Battery sub-healthy state type II is a single cell voltage, and the average voltage of the battery pack difference is large and partly outside the  $\pm 3\sigma$  range. To show this inconsistency, the area differential method calculates the area enclosed by the single battery's voltage and the average voltage of the battery pack within the selected time. The calculation formula is as follows:

$$A_{diff} = \sum |(x_{i,j} - \mu_i)|, \quad (14)$$

where  $A_{diff}$  is the differential area in the selected time period.

## 3.2. Identification of Sub-Health Status Type I

### 3.2.1. ICC Calculation of Sub-Health State Type

Sub-health state type I indicates that the voltage of the single battery is inconsistent with the overall voltage of the battery pack, and the ICC principle can be used to identify it. The ICC calculations for the voltage of single cell No. 1 are as follows:

$$C = \frac{(\sum x)^2}{N} = \frac{0.01236}{358} = 3.4545 \times 10^{-5} \quad (15)$$

$$SS_{bl} = \sum_{i=1}^b \frac{\left( \sum_{j=1}^k x_{ij} \right)^2}{k} - C = 4.1430 \times 10^{-2} - 3.4545 \times 10^{-5} = 4.1395 \times 10^{-2} \quad (16)$$

$$SS_{tr} = \sum_{j=1}^k \frac{\left( \sum_{i=1}^b x_{ij} \right)^2}{b} - C = 4.0253 \times 10^{-5} - 3.4545 \times 10^{-5} = 5.7085 \times 10^{-6},$$

$$SS_{er} = \sum x^2 - SS_{bl} - SS_{tr} - C = 6.3644 \times 10^{-2} - 4.1395 \times 10^{-2} - 5.7085 \times 10^{-6} - 3.4545 \times 10^{-5} = 2.2209 \times 10^{-2}$$

$$MS_{er} = \frac{SS_{er}}{v_{er}} = \frac{2.2209 \times 10^{-2}}{178} = 1.2478 \times 10^{-4}$$

$$MS_{bl} = \frac{SS_{bl}}{v_{bl}} = \frac{4.140 \times 10^{-2}}{179} = 2.3256 \times 10^{-4}$$

$$ICC = \frac{\frac{MS_{bl} - MS_{er}}{m}}{\frac{MS_{bl} - MS_{er}}{m} + MS_{er}} = \frac{5.389 \times 10^{-5}}{1.7867 \times 10^{-4}} = 0.3016$$

Based on Formula (1), the *ICC* of the voltage of battery No. 1 is 0.3016; the *ICC* of each single battery voltage was calculated using analogy, as shown in Figure 3. It can be concluded from Figure 1 that since battery No. 1 has sub-health state type I, the calculated *ICC* is lower, while the *ICC* of single battery No. 53 without a sub-health state is 0.85, as shown in the blue graph in Figure 3, which is significantly greater than that of single battery No. 1. At this time, as shown in the green graph in Figure 3, not only is the *ICC* of battery No. 1's voltage low, but the *ICCs* of the voltages of cells No. 12 and 92 are also relatively low. From Figure 4, it can be concluded that both batteries have sub-health state type I.

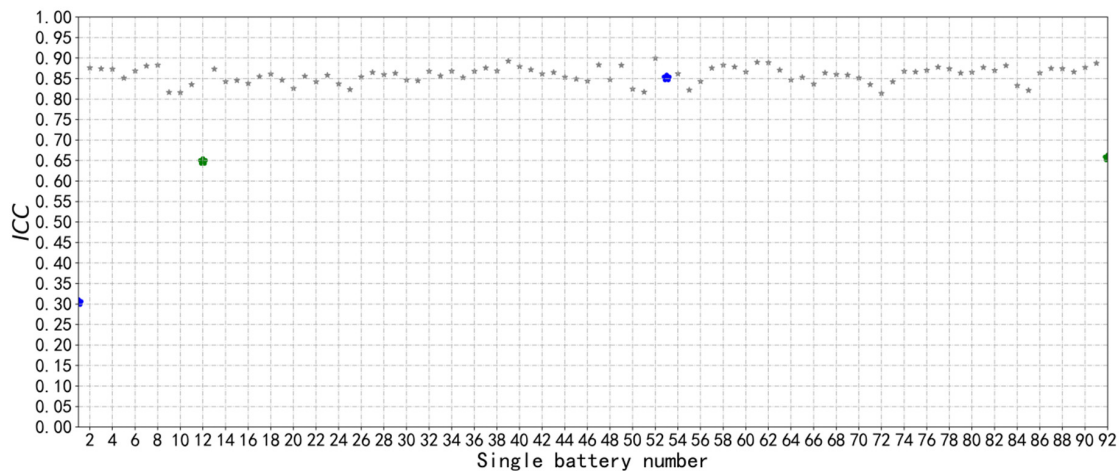


**Figure 3.** The *ICCs* of different cells' voltages.

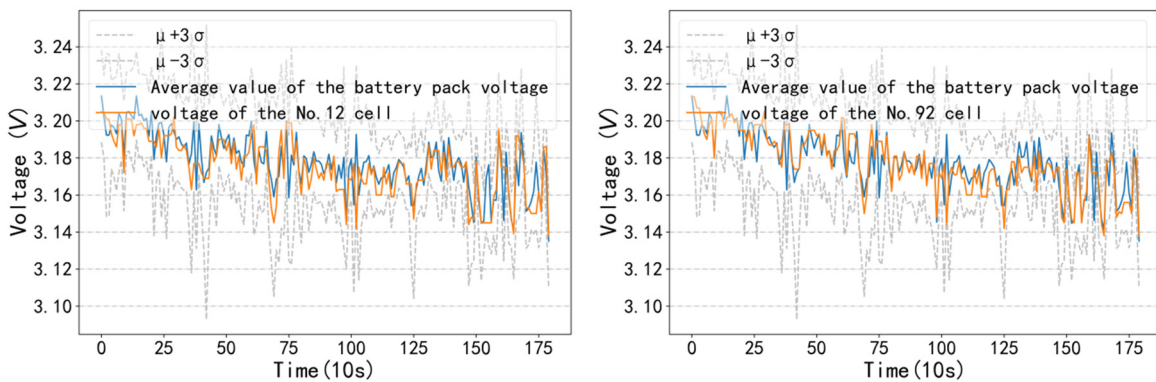


**Figure 4.** Graphs of the voltage of single batteries over time.

### 3.2.2. Threshold Calculation of Sub-Health State Type I

Usually, the *ICC* ranges from 0.75 to 1. When the *ICC* < 0.75, it is considered that the two groups of data are inconsistent; on the contrary, when the *ICC* > 0.75, it is considered that the two groups of data are consistent. Due to the consistency of the time series of single batteries, the *ICCs* of  $V_{j,diff}$  and  $\bar{V}_{diff}$  are both higher. Using a threshold of 0.75 as the criterion to determine the sub-health state does not match the actual characteristics of the battery voltage data. Therefore, this paper uses vehicle operation data under different working conditions to determine the threshold value. Figure 5 shows a box diagram of the *ICCs* of vehicles under different working conditions. We divided the one-month operation data of 72 vehicles at fixed time intervals and calculated the *ICC* value of each section

of data. The figure shows that the lower limit of the box diagram of the 72 vehicles is distributed above 0.7.

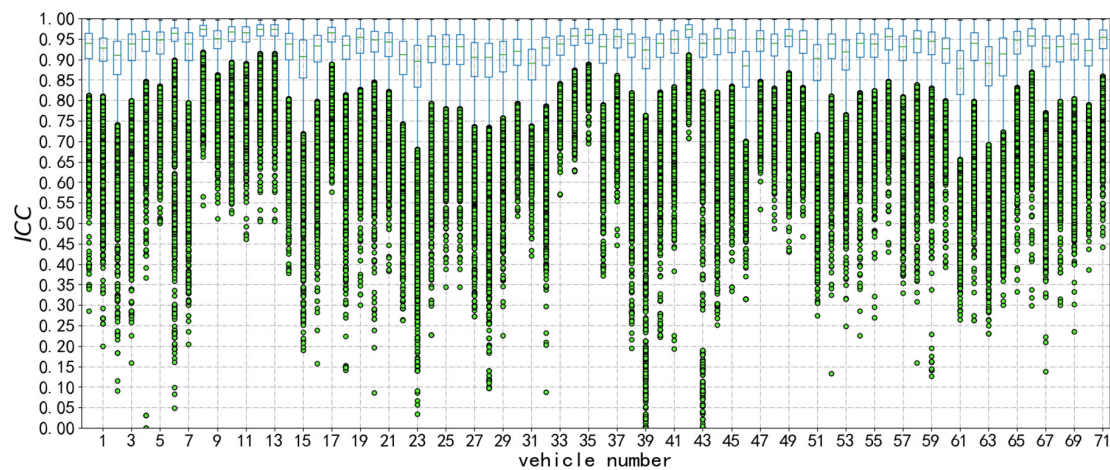


**Figure 5.** Box plot of ICCs of different vehicles.

Box plots can not only observe the distribution of data but can also be used to remove outliers. Up to more than 90 percent of the data is contained between the upper and lower limits in the box plot, so the lower limit can be used as a threshold to remove abnormal data. Since the amount of data in the sub-health state is only a small part of the overall data volume, the lower limit can also be used as the identification criterion for the sub-health state. Although the lower limit values under different working conditions are above 0.7, the specific values are different, and for the reliability of the threshold selection, the lower limit values of the box plots under different working conditions are summarized in Figure 6. We used the lower limit of 0.805 as the ICC threshold. When the ICC value is lower than the threshold, it is determined that the single battery is in a sub-health state.

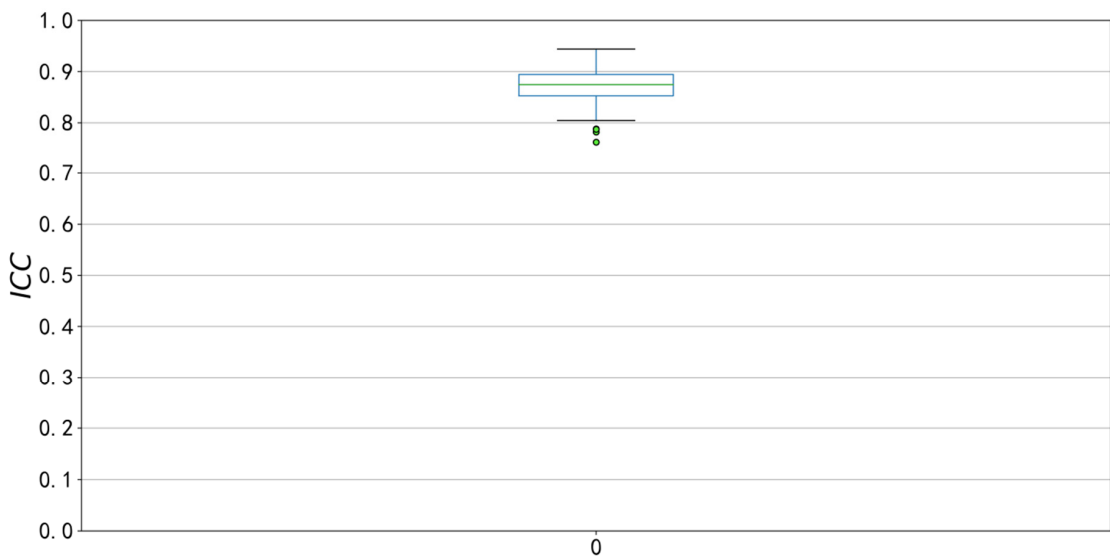


**Figure 6.** Box plot of ICC of general vehicles.

### 3.3. Identification of Sub-Health State Type II

#### 3.3.1. Z-Score Calculation for Sub-Health Type II

The calculation process for the voltage Z-score of cell No. 1 at a certain time is as follows:

$$\mu_i = \frac{1}{n} \sum_{j=1}^n (x_{i,j}) = \frac{1}{98} \sum_{j=1}^{98} (x_{i,j}) = 3.188$$

$$\sigma_i = \sqrt{\frac{1}{n} \left[ \sum_{j=1}^n (x_{i,j} - \mu_j)^2 \right]} = 0.01$$

$$Z_{i,1} = \frac{x_{i,1} - \frac{1}{n} \sum_{j=1}^n (x_{i,j})}{\sqrt{\frac{1}{n} \left[ \sum_{j=1}^n (x_{i,j} - \mu_i)^2 \right]}} = \frac{3.183 - 3.188}{0.01} = -0.5$$

According to Formula (13), the Z-score of the voltage of single cell No. 1 is  $-0.5$ . The Z-score of each single cell voltage was calculated using analogy, as shown in Figure 7. Since the driver's emergency operation during the actual operation of the vehicle may cause the voltage to rise temporarily, the instantaneous cell voltage Z-score cannot fully reflect the battery status, so real-time monitoring voltage data over a certain period were selected to calculate the Z-score box chart, as shown in Figure 8. The figure shows that the Z-scores of the voltage of single cells No. 11 and 14 clearly deviate from the Z-score of the overall voltage of the battery pack; therefore, the two single cells may be in sub-health state.

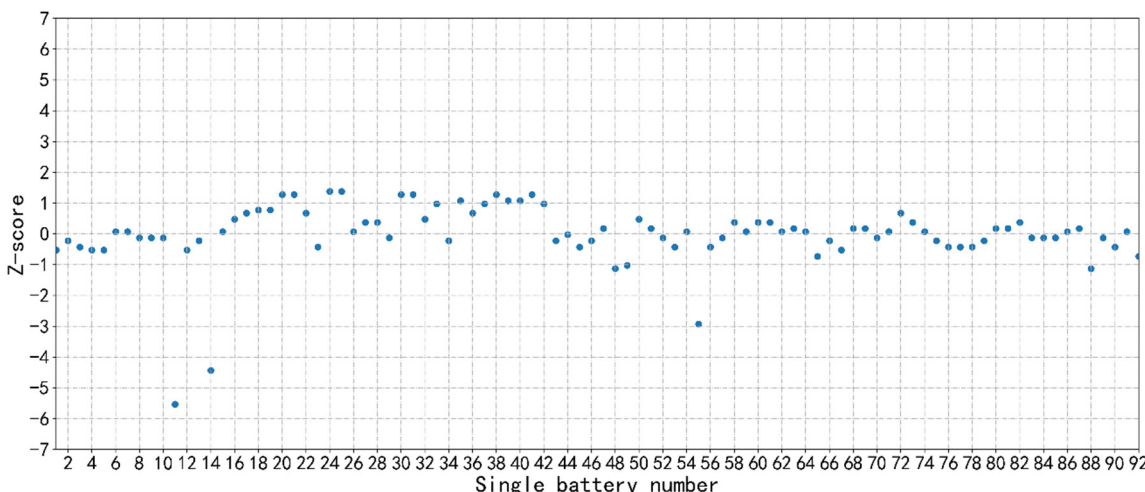


**Figure 7.** Z-score scatter graph of instantaneous voltage of single cells.

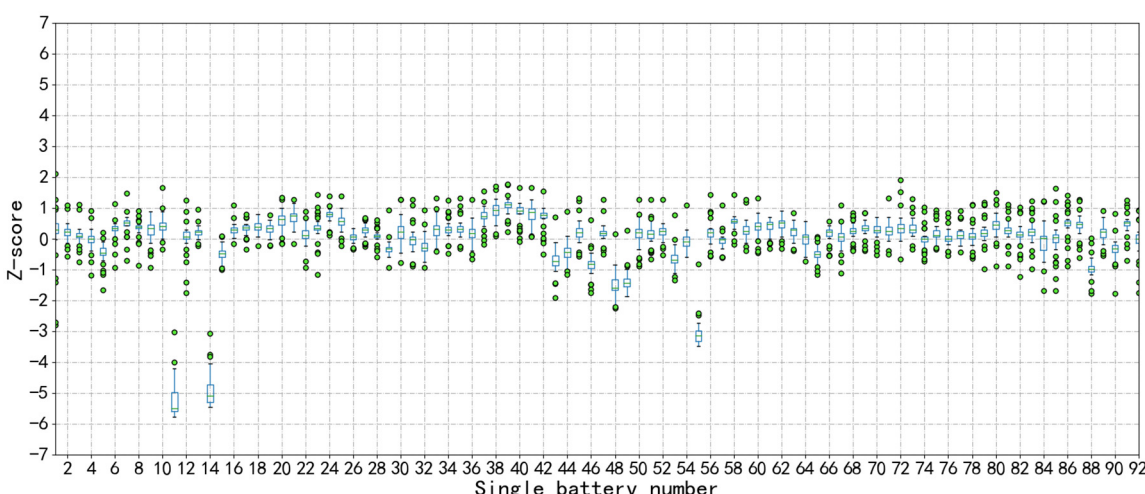


**Figure 8.** Box plot of Z-score of single battery voltage.

### 3.3.2. Calculation of Sub-Health Type II by Differential Area Method

In order to eliminate the instantaneous increase in voltage caused by the driver's emergency operation, the differential area method was introduced to quantitatively describe sub-health state type II. The further the single cell voltage deviates from the average value of the cell pack voltage, the larger the differential area will be. This method can not only determine the number of single batteries in the sub-health state, but also avoids the misjudgment caused by the temporary rise in the voltage at a certain moment.

$$A_{diff} = \sum_{i=1}^{30} |(x_{i,1} - \mu_i)| = 0.272$$

Based on Formula (14), the differential area of battery No. 1 is 0.272. The differential area of each single battery voltage was calculated using analogy, as shown in Figure 9. It can be concluded from Figure 2 that since battery No. 11 has a type II sub-health state, the calculated differential area is 1.82. However, as shown in the blue graph in Figure 3, the voltage differential area of battery No. 4 without sub-health status is 0.07, which is significantly smaller than that of battery No. 11, as shown in the green graph in Figure 3. Except for the higher differential area of battery No. 11 at this moment, the voltage differential area of single batteries No. 14 and 55 are both higher. As shown in Figure 10, the voltage of the single cell battery changes with time, and it can be concluded that the two single cells No. 14 and No. 55 are in the type II sub-health state.

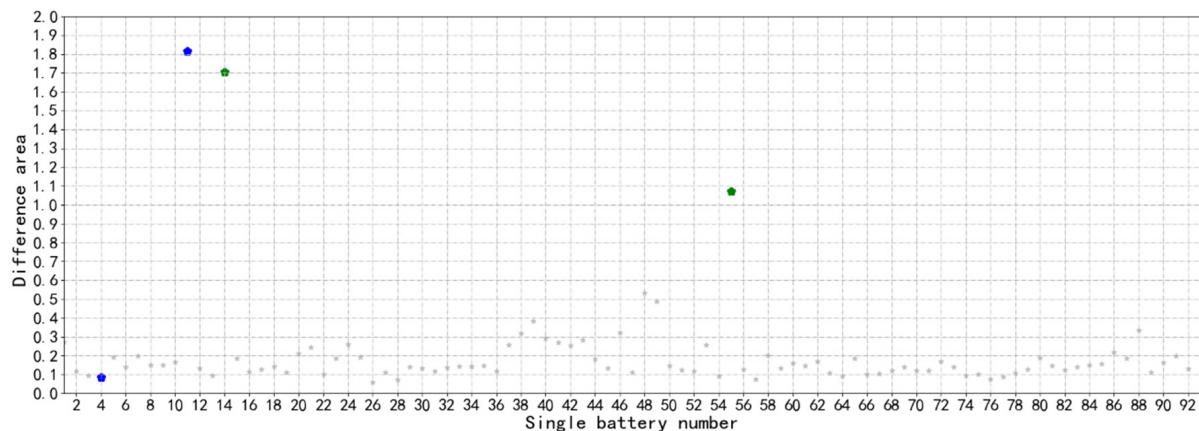


**Figure 9.** Differential area of single battery voltage.

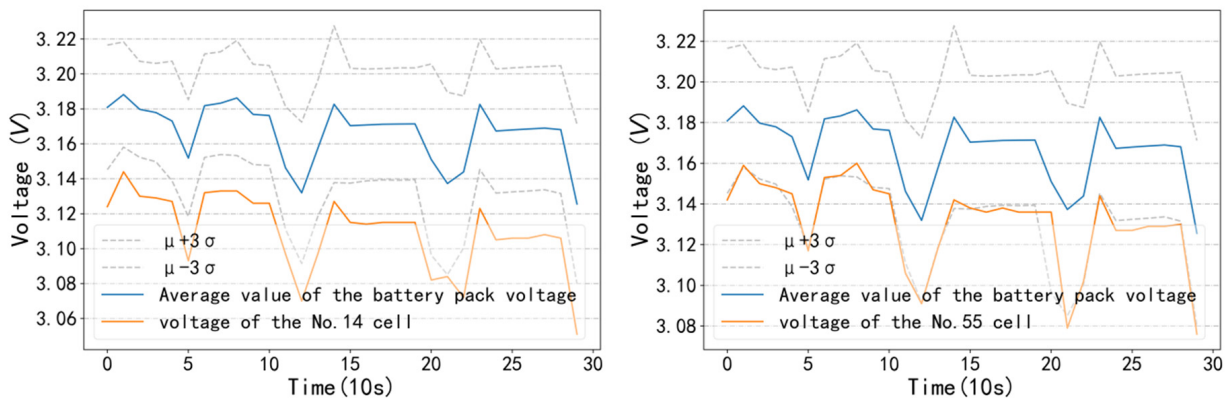


**Figure 10.** Graph of the voltage of single batteries over time.

### 3.3.3. Threshold of Sub-Health State Type II Based on the $3\delta$ Rule

For sub-health state type II, although the differential area method and Z-score can be used to compare the discreteness of each single battery clearly, it is possible to judge which battery is more prone to the trend of entering a sub-health state. However, a unified threshold cannot be given to determine whether a single battery is in a sub-health state. In order to solve this problem, this paper introduces the  $3\delta$  rule on the basis of the Z-score and differential area method to judge sub-health state type II. Figure 11 is a scatter plot of the differential area Z-score. From the figure, it can be concluded that the Z-scores of the voltages of cells No. 11, 14, and 55 were all greater than three. According to the principle of the  $3\delta$  rule, these three single cells were in a sub-health state.

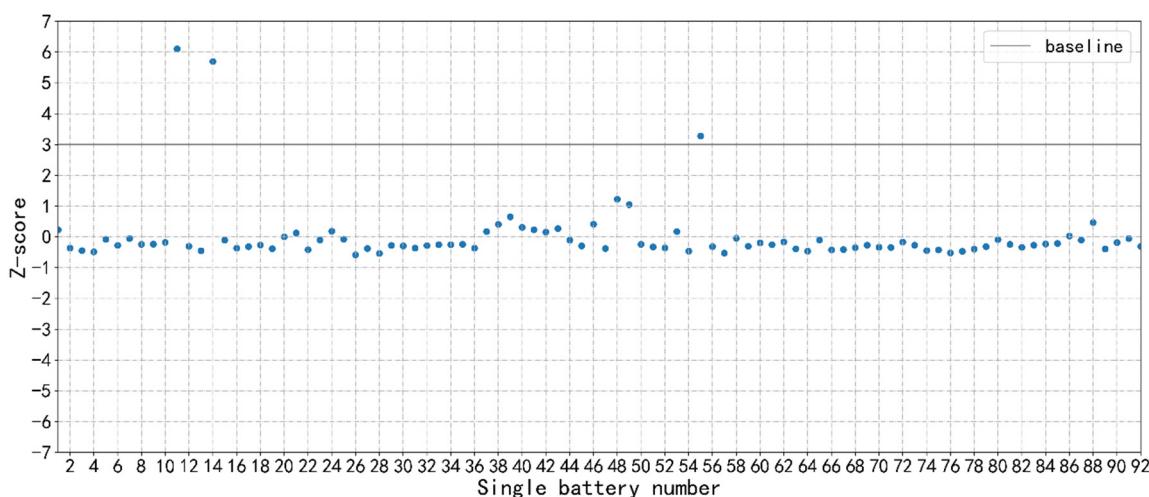


**Figure 11.** Scatter plot of Z-score of differential area.

## 4. Method Verification

### 4.1. Verification Methods for Sub-Health State Type I

In order to verify the feasibility of the ICC method, we selected the data of other vehicles to calculate the ICC values of the single battery voltages, as shown in Figure 12. It can be seen from the figure that the ICCs of single cells No. 33, 34, 35, 36, and 82 were all lower than the threshold. We then drew a graph of the changes of these cells over time to determine whether the sub-health state type I was satisfied. At the same time, cell No. 1 with an ICC greater than the threshold was selected as the control. As shown in Figure 13, cells No. 33, 34, 35, 36, and 82 were in a sub-health state.

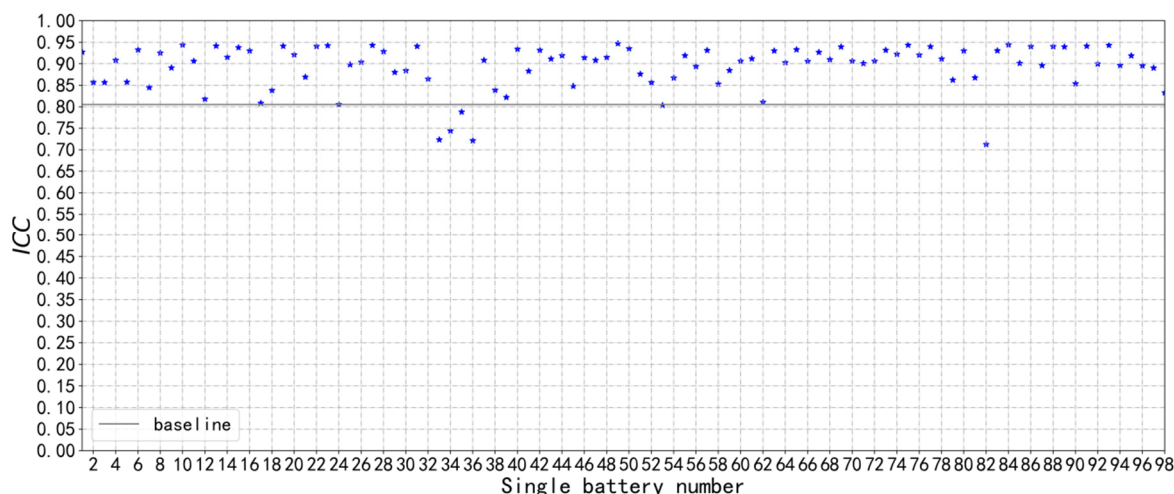


**Figure 12.** The ICCs of different cell voltages.

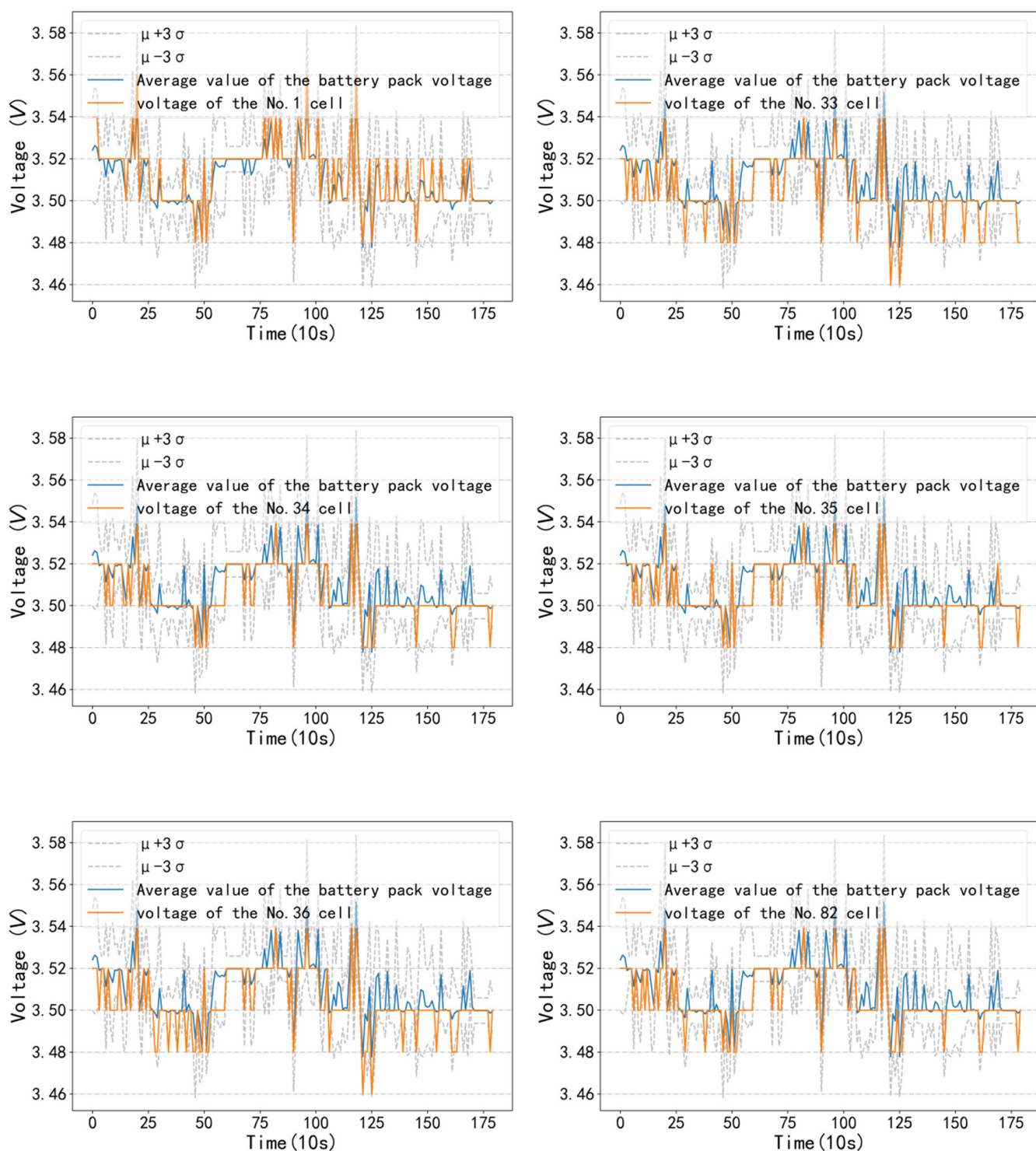


**Figure 13.** Graphs of the voltage of single batteries over time.

In the repeated operation of the vehicle, a single sub-health state cannot reflect the health of the battery. Therefore, it was necessary to calculate the frequency of the sub-health state of the single batteries in each vehicle for one month. From the frequency chart of sub-health state type I of single batteries in Figure 14, it can be seen that cells No. 33 and 70 had a higher frequency of sub-health state type I; in particular, for single battery No. 70, the frequency of a sub-health state within one month was close to 0.5.

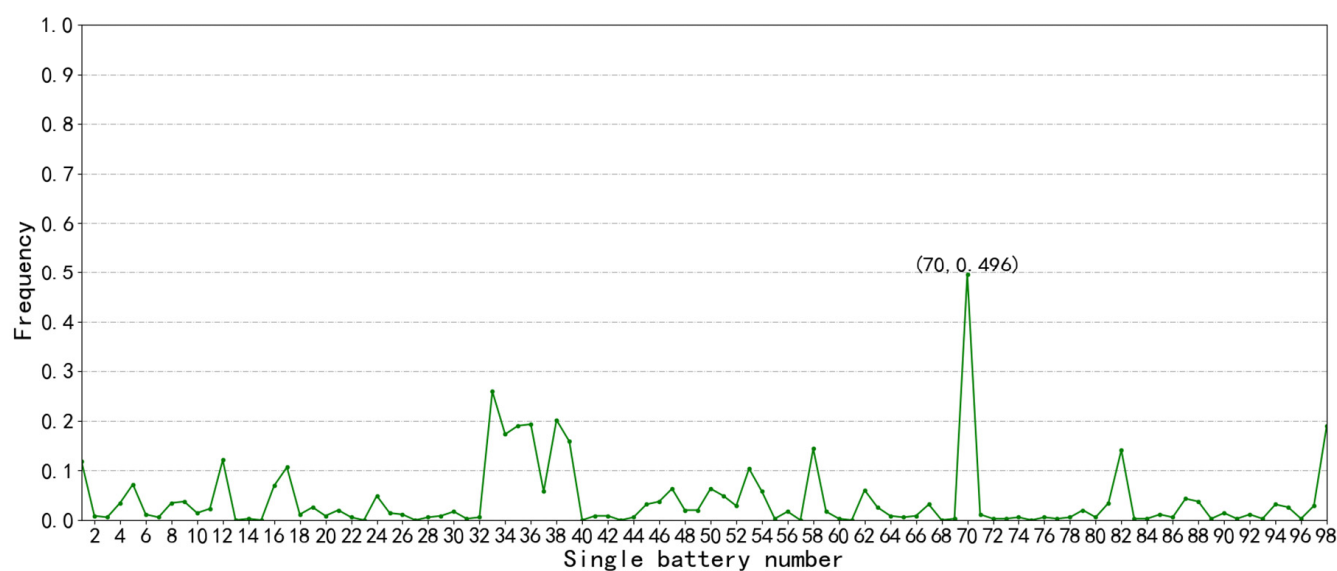


**Figure 14.** Frequency graph of sub-health state type I of single cells.

#### 4.2. Verification Methods for Sub-Health State Type II

In order to verify the feasibility of the method of sub-health state type II, the data of other vehicles were selected to calculate the Z-scores of the differential area of single battery voltages, as shown in Figure 15. The figure shows that the Z-scores of the differential area of the voltage of single cells No. 14, 26, 34, and 97 were greater than three. We drew a graph of the voltage changes of these single batteries over time to determine whether the sub-health state type II was satisfied. At the same time, cells No. 1 and 2 with Z-scores of differential areas lower than three were selected as the control. As shown in Figure 16, a sub-health state occurred in cells No. 14, 26, 34, and 97.

Similar to sub-health state type I, we drew a frequency chart of the sub-health state of the single batteries within one month, as shown in Figure 17. From the figure, it can be seen that the frequency of sub-health state type II in cells No. 26 and 97 is higher, both exceeding 0.5.

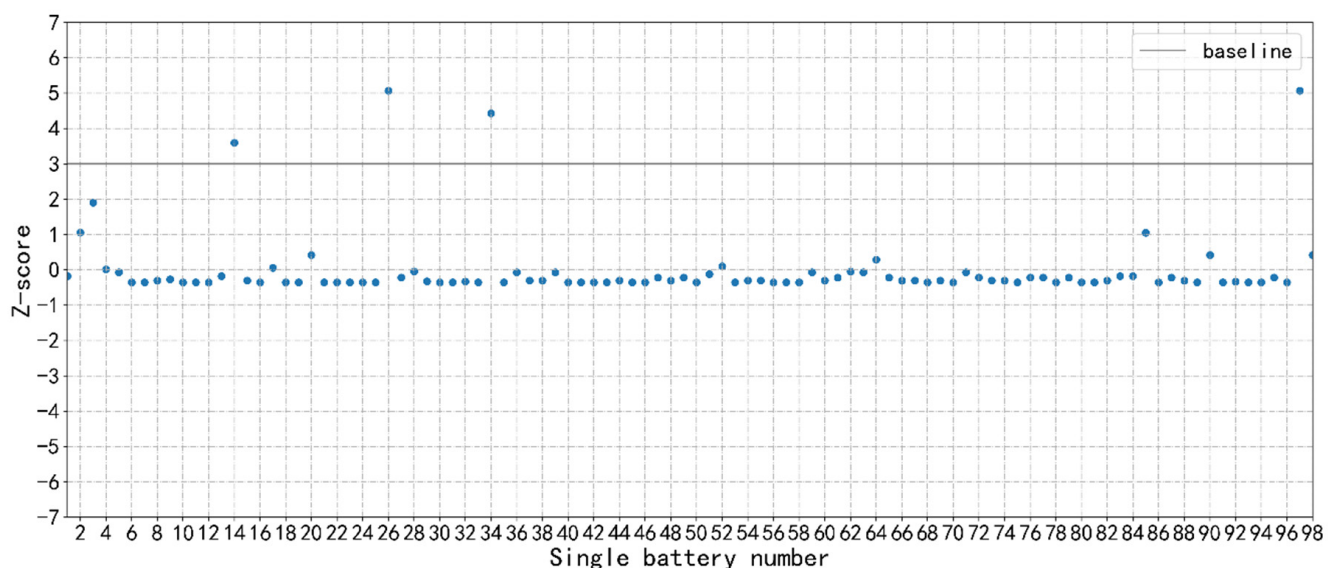


**Figure 15.** Z-scores of differential area of cell voltages.

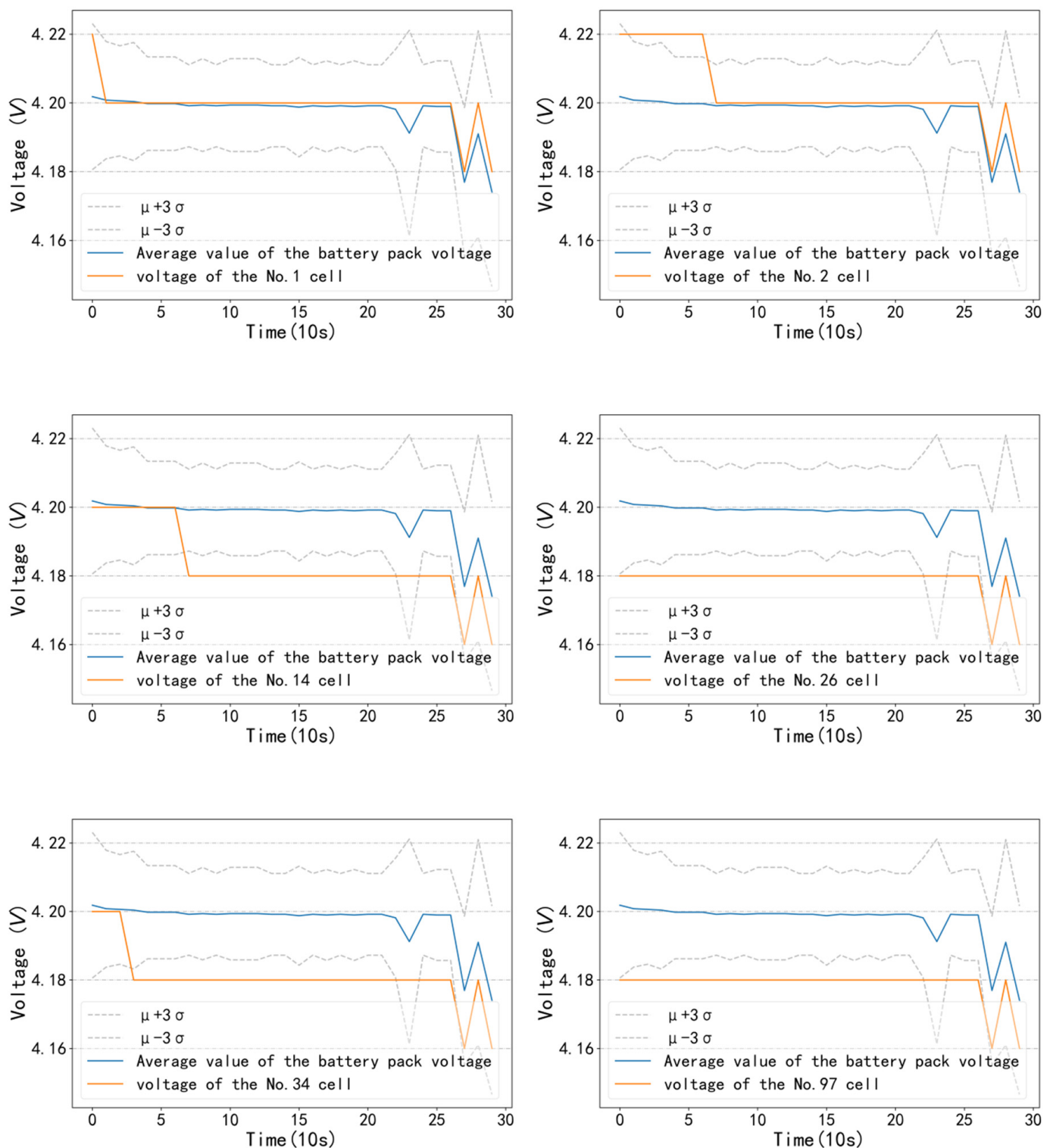


**Figure 16.** Graphs of the voltage of single batteries over time.

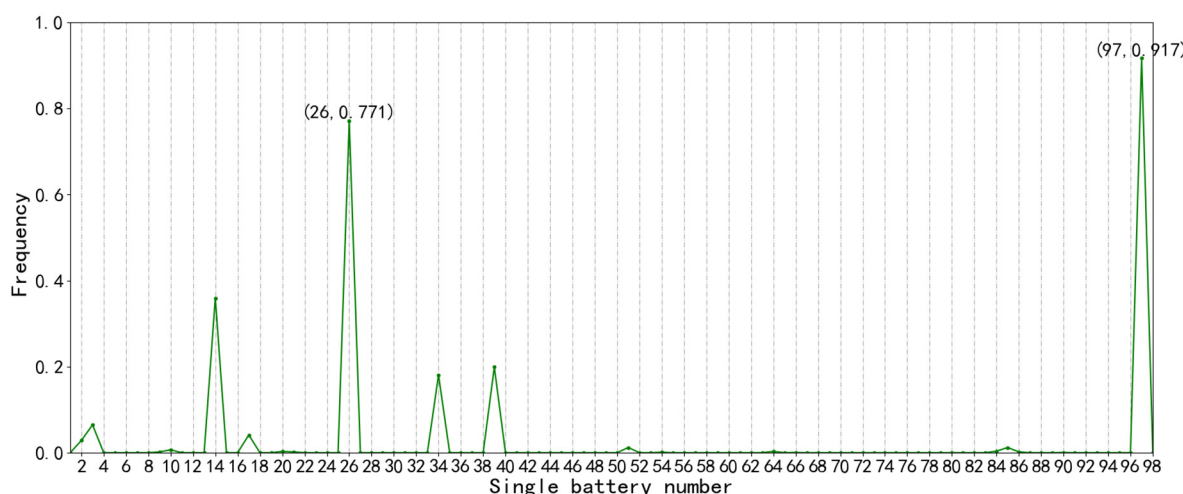


**Figure 17.** Frequency graph of sub-health state type II of single cells.

## 5. Conclusions

This paper proposes two different methods to identify two typical battery sub-health states. Based on the inconsistency between the voltage of a single cell and the overall voltage of the battery pack, the *ICC* method was proposed, and the *ICC* threshold value of 0.805 was used as the criterion for judging the sub-health state based on the operating data of each vehicle under different working conditions. Based on the problem of the voltage of a single cell deviating from the overall voltage of the battery pack, the differential area method and the Z-score method were combined, and according to the  $3\sigma$  rule, a threshold of three was used as the standard for determining the sub-health state by the Z-score of the differential area.

Since a single sub-health state cannot fully reflect the overall health of the battery, it is necessary to calculate the monthly sub-health state frequency of each vehicle's single battery and to take a single battery with high frequency as the focus of vehicle operation in the future.

**Author Contributions:** Supervision, W.G. and J.T.; formal analysis, C.Y., W.G. and J.T.; visualization, C.Y., W.G. and J.T.; validation, C.Y.; writing—review and editing, C.Y., W.G. and C.W.; data curation, C.W. and Z.W.; resources, C.W. and Z.W.; writing—original draft preparation, C.Y., W.G. and J.T. All authors have read and agreed to the published version of the manuscript.

**Funding:** This research was funded by the National Key Research and Development Program of China (2018YFB1601100); National Key Research and Development Plan, research on charging infrastructure optimization based on large-scale application of electric vehicles (2018YFE0105100); R&D Program of Beijing Municipal Education Commission (KM202010009007); Youth Top Talent Training Program of Beijing Municipal Education Commission (CIT&TCD201804006).

**Institutional Review Board Statement:** Not applicable.

**Informed Consent Statement:** Not applicable.

**Data Availability Statement:** The case data of the vehicle voltages are from the official websites of the relevant institutions. The vehicle voltage data used in this article are from the New Energy Vehicle National Big Data Alliance Open Lab, which is an online data platform that cannot be shared, and we currently do not have login access. Although we cannot share vehicle voltage data, we present the results of the analysis of the data in this paper.

**Conflicts of Interest:** The authors declare no conflict of interest.

## Abbreviations

### Nomenclature variable

$V_{j,diff}$	The difference in voltage of a single cell at adjacent time points in the $j$ -th column
$\bar{V}_{diff}$	Difference between the average values of cell pack voltage at adjacent time points
$MS_{er}$	Mean square error of the error term between $V_{j,diff}$ and $\bar{V}_{diff}$
$MS_{bl}$	The mean square error of the block term between $V_{j,diff}$ and $\bar{V}_{diff}$
$SS_{er}$	Sum of squares of deviation from mean of the error term between $V_{j,diff}$ and $\bar{V}_{diff}$
$SS_{bl}$	Sum of squares of deviation from mean of the block term between $V_{j,diff}$ and $\bar{V}_{diff}$
$SS_{tr}$	Sum of squares of deviation from mean of the treatment term between $V_{j,diff}$ and $\bar{V}_{diff}$
$v_{bl}$	The degree of freedom of the block term between $V_{j,diff}$ and $\bar{V}_{diff}$
$v_{er}$	The degree of freedom of the error term between $V_{j,diff}$ and $\bar{V}_{diff}$
$k$	The number of treatment groups between $V_{j,diff}$ and $\bar{V}_{diff}$
$b$	The number of blocks between $V_{j,diff}$ and $\bar{V}_{diff}$
$C$	Correction coefficient between $V_{j,diff}$ and $\bar{V}_{diff}$
$N$	Total number of data points between $V_{j,diff}$ and $\bar{V}_{diff}$
$Z_{i,j}$	The $i$ -th time point and the $j$ -th Z-score of single battery voltage
$x_{i,j}$	The $i$ -th time point and the $j$ -th single battery voltage
$\mu_j$	The $i$ -th time point average value of battery pack voltage
$\sigma_j$	The $i$ -th time point standard deviation of battery pack voltage

### Subscripts

diff	Difference
er	Error
bl	Block
tr	Treatment

### Acronyms

ICC	Interclass correlation coefficient
EVs	Electric vehicles
BMS	Battery management system
C	Capacity

## References

- Zhang, S.; Xiong, R.; Gao, J. Battery durability and longevity based power management for plug-in hybrid electric vehicle with hybrid energy storage system. *Appl. Energy* **2016**, *179*, 316–328. [[CrossRef](#)]
- Merkle, L.; Pthig, M.; Schmid, F. Estimate e-Golf Battery State Using Diagnostic Data and a Digital Twin. *Batteries* **2021**, *7*, 15. [[CrossRef](#)]
- Pearre, N.S.; Kempton, W.; Guensler, L.R.; Elango, V.V. Electric vehicles: How much range is required for a day's driving. *Transp. Res. Part C Emerg. Technol.* **2011**, *19*, 1171–1184. [[CrossRef](#)]
- Li, X.; Zhao, J.; Duan, J.; Panchal, S.; Yuan, J.; Fraser, R.; Fowler, M.; Chen, M. Simulation of cooling plate effect on a battery module with different channel arrangement. *J. Energy Storage* **2022**, *49*, 104113. [[CrossRef](#)]
- Chen, Z.; Li, X.; Shen, J.; Yan, W.; Xiao, R. A Novel State of Charge Estimation Algorithm for Lithium-ion Battery Packs of Electric Vehicles. *Energies* **2016**, *9*, 710. [[CrossRef](#)]
- Dubarry, M.; Vuillaume, N.; Liaw, B.Y. From single cell model to battery pack simulation for Li-ion batteries. *J. Power Sources* **2009**, *18*, 500–507. [[CrossRef](#)]
- Li, X.; Zhang, X.; Zhou, Y. Power battery fault diagnosis system based on fuzzy neural network. *Chin. J. Power Sources* **2019**, *43*, 1391–1394.
- Baronti, F.; Roncella, R.; Saletti, R. Performance comparison of active balancing techniques for lithium-ion batteries. *J. Power Sources* **2014**, *267*, 603–609. [[CrossRef](#)]
- Rafael, C.; Frederic, H.; Peter, B. Methodology for Determining Time-Dependent Lead Battery Failure Rates from Field Data. *Batteries* **2021**, *7*, 39. [[CrossRef](#)]
- Wu, C.; Zhu, C.; Ge, Y.; Zhao, Y. A review on fault mechanism and diagnosis approach for Li-ion batteries. *J. Nanomater.* **2015**, *2015*, 8. [[CrossRef](#)]
- Tran, M.-K.; Panchal, S.; Khang, T.D.; Panchal, K.; Fraser, R.; Fowler, M. Concept Review of a Cloud-Based Smart Battery Management System for Lithium-Ion Batteries: Feasibility, Logistics, and Functionality. *Batteries* **2022**, *8*, 19. [[CrossRef](#)]
- Zhao, R.; Liu, J.; Gu, J. Simulation and experimental study on lithiumion battery short circuit. *Appl. Energy* **2016**, *173*, 29–39. [[CrossRef](#)]
- Dey, S.; Biron, Z.A.; Tatipamula, S.; Das, N.; Mohon, S.; Ayalew, B.; Pisu, P. On-board Thermal Fault Diagnosis of Lithium-ion Batteries for Hybrid Electric Vehicle Application. *IFAC Pap.* **2015**, *2015*, 389–394. [[CrossRef](#)]

14. Yao, L.; Xiao, Y.; Gong, X.; Hou, J.; Chen, X. A novel intelligent method for fault diagnosis of electric vehicle battery system based on wavelet neural network. *J. Power Sources* **2020**, *453*, 227870. [[CrossRef](#)]
15. Chen, Z.; Xiong, R.; Tian, J.; Shang, X.; Liu, J. Model-based fault diagnosis approach on external short circuit of lithium-ion battery used in electric vehicles. *Appl. Energy* **2016**, *184*, 365–374. [[CrossRef](#)]
16. Dey, S.; Biron, Z.A.; Tatipamula, S.; Das, N.; Mohon, S.; Ayalew, B.; Pisu, P. Model-based real-time thermal fault diagnosis of Lithium-ion batteries. *Control. Eng. Pract.* **2016**, *56*, 37–48. [[CrossRef](#)]
17. Han, B.; Wang, D.; Li, S. Research on battery connection reliability based on DC internal resistance. *Chin. J. Power Sources* **2017**, *41*, 981–983.
18. Xia, B.; Chen, Z.; Mi, C.; Robert, B. External short circuit fault diagnosis for lithium-ion batteries. In Proceedings of the Transportation Electrification Conference and Expo (ITEC), Dearborn, MI, USA, 15–18 June 2014; pp. 1–6. [[CrossRef](#)]
19. Chen, W.; Chen, W.-T.; Saif, M.; Li, M.-F.; Wu, H. Simultaneous fault isolation and estimation of lithium-ion batteries via synthesized design of luenberger and learning observers. *IEEE Trans. Control. Syst. Technol.* **2014**, *22*, 290–298. [[CrossRef](#)]
20. Xu, J.; Liang, D.; Wei, G.; Zhu, C. Series battery pack’s contact resistance fault diagnosis analysis. *Trans. China Electrotech. Soc.* **2017**, *32*, 106–112. [[CrossRef](#)]
21. Sidhu, A.; Izadian, A.; Anwar, S. Adaptive Nonlinear Model-Based Fault Diagnosis of Li-ion Batteries. *IEEE Trans. Ind. Electron.* **2014**, *62*, 1002–1011. [[CrossRef](#)]
22. Liu, Z.; He, H. Model-based Sensor Fault Diagnosis of a Lithium-ion Battery in Electric Vehicles. *Energies* **2015**, *6*, 6509–6527. [[CrossRef](#)]
23. Dey, S.; Mohon, S.; Pisu, P.; Ayalew, B. Sensor fault detection, isolation, and estimation in lithium-ion batteries. *IEEE Trans. Control. Syst. Technol.* **2016**, *24*, 2141–2149. [[CrossRef](#)]
24. Tran, M.-K.; Cunanan, C.; Panchal, S.; Fraser, R.; Fowler, M. Investigation of Individual Cells Replacement Concept in Lithium-Ion Battery Packs with Analysis on Economic Feasibility and Pack Design Requirements. *Processes* **2021**, *9*, 2263. [[CrossRef](#)]
25. Chen, Z.; Zheng, C.; Lin, T.; Yang, Q. Multifault Diagnosis of Li-Ion Battery Pack Based on Hybrid System. *IEEE Trans. Transp. Electrif.* **2022**, *8*, 1769–1784. [[CrossRef](#)]
26. Hu, J.; He, H.; Wei, Z.; Li, Y. Disturbance-immune and aging-robust internal short circuit diagnostic for lithium-ion battery. *IEEE Trans. Ind. Electron.* **2021**, *69*, 1988–1999. [[CrossRef](#)]
27. Hong, J.; Wang, Z.; Yao, Y. Fault prognosis of battery system based on accurate voltage abnormality prognosis using long short-term memory neural networks. *Appl. Energy* **2019**, *5*, 113381. [[CrossRef](#)]
28. Yang, R.; Xiong, R.; He, H.; Chen, Z. A fractional-order model-based battery external short circuit fault diagnosis approach for all-climate electric vehicles application. *J. Clean. Prod.* **2018**, *187*, 950–959. [[CrossRef](#)]
29. Gao, Z.; Cheng, C.S.; Woo, W.L.; Jia, J.; Wei, D.T.W. Genetic algorithm based back-propagation neural network approach for fault diagnosis in lithium-ion battery system. In Proceedings of the 6th International Conference on Power Electronics Systems and Applications, Hong Kong, China, 15–17 December 2015. [[CrossRef](#)]
30. Xia, F.; Ma, X.; Luo, Z.; Zhang, H.; Sun, P. Application of improved D-S evidence theory in fault diagnosis of lithium batteries in electric vehicles. *CAAI Trans. Intell. Syst.* **2017**, *12*, 526–537. [[CrossRef](#)]
31. Li, X.; Wang, Z. A novel fault diagnosis method for lithium-Ion battery packs of electric vehicles. *Measurement* **2018**, *10*, 402–411. [[CrossRef](#)]
32. Xue, Q.; Li, G.; Zhang, Y.; Shen, S.; Chen, Z.; Liu, Y. Fault diagnosis and abnormality detection of lithium-ion battery packs based on statistical distribution. *J. Power Sources* **2021**, *482*, 228964. [[CrossRef](#)]
33. Zou, D.; Chen, H.; Li, X.; Lu, Y.; Huang, P. Consistency evaluation method of lithium battery pack based on cloud charging data. *Power Grid Technol.* **2022**, *2022*, 308. [[CrossRef](#)]
34. Dai, H.F.; Wang, N.; Wei, X.Z.; Sun, Z.C.; Wang, J.Y. A review of the research on monomer inconsistency of automotive power lithium-ion batteries. *Automot. Eng.* **2014**, *36*, 181–188. [[CrossRef](#)]
35. Kumro, F.G.; Smith, F.M.; Yallop, M.J.; Ciernia, L.A.; Lucy, M.C. Estimates of intra- and interclass correlation coefficients for rump touches and the number of steps during estrus in postpartum cows. *J. Dairy Sci* **2020**, *104*, 2318–2333. [[CrossRef](#)]
36. Zidan, M.; Thomas, R.L.; Slovis, T.L. What you need to know about statistics, part II: Reliability of diagnostic and screening tests. *Pediatr. Radiol.* **2015**, *45*, 317–328. [[CrossRef](#)] [[PubMed](#)]
37. Post, M.W. What to do with “Moderate” reliability and validity coefficients? *Arch. Phys. Med. Rehabil.* **2016**, *97*, 1051–1052. [[CrossRef](#)] [[PubMed](#)]